First results on a sensor bio-inspired by electric fish

Noël Servagent, Brahim Jawad, Stéphane Bouvier, Frédéric Boyer, Alexis Girin, Francesco Gomez, Vincent Lebastard, Pol-Bernard Gossiaux

Noël Servagent, Brahim Jawad, Stéphane Bouvier, Frédéric Boyer, Alexis Girin, et al.. First results on a sensor bio-inspired by electric fish. 2012. hal-00695453

HAL Id: hal-00695453
https://hal.science/hal-00695453
Submitted on 9 May 2012

First results on a sensor bio-inspired by electric fish

Noël Servagent[1], Brahim Jawad[1,2], Stéphane Bouvier[1], Frédéric Boyer[2],
Alexis Girin[2], Francesco Gomez[1], Vincent Lebastard[2], and Pol-Bernard Gossiaux[1].

[1] SUBATECH UMR CNRS 6457,
Laboratoire de Physique Subatomique et des Technologies Associées
University of Nantes - IN2P3/CNRS - Ecole des Mines de Nantes
4 rue Alfred Kastler, 44072 Nantes Cedex 03, France

[2] Ecole des Mines de Nantes, IRCCYN UMR CNRS 6597
1, rue de la Noë, BP 92101, 44321 NANTES Cedex 03, France

8 mai 2012

Résumé

This article presents the first results of a work which aims at designing an active sensor inspired by the electric fish. Its interest is its potential for robotics underwater navigation and exploration tasks in conditions where vision and sonar would meet difficulty. It could also be used as a complementary omnidirectional, short range sense to vision and sonar. Combined with a well defined engine geometry, this sensor can be modeled analytically. In this article, we focus on a particular measurement mode where one electrode of the sensor acts as a current emitter and the others as current receivers. In spite of the high sensitivity required by electric sense, the first results show that we can obtain a detection range of the order of the sensor length, which suggests that this sensor principle could be used in future for robotics obstacle avoidance.

1 Introduction

Underwater robot navigation is essentially based on the use of vision and sonar. While the range of vision decreases with the rarefaction of available light energy, sonar escapes this constraint, since, as any active sense, the energy supporting the measured information (here acoustic) is produced by the sensor itself. Exploited by swimming animals practicing echolocation, this advantage makes sonar a solution ideally suited to underwater robot navigation in dark open spaces. On the other hand, in highly confined spaces, such as narrow pipes and tunnels, caves and shallow waters, the reverberation of multiple echoes from the obstacles can make the interpretation of acoustic measurements difficult. Furthermore, when waters contain a lot of floating particles, diffraction can jam the sonar signals. Thus, in the navigation of complex environments immersed in turbid waters, an alternative sense would be of great assistance to vision and sonar. In fact, nature has already invented such a sense, the electric sense, which is used for navigation and communication by several families of fish. These electric fish are principally nocturnal and live in the particle rich waters of the equatorial forests [1]. These fish are able to navigate in the complete darkness of their natural habitat using self generated electrical fields. They emit electric signals into the environment, which in turn are perceived using an array of electroreceptor organs in their skin. This ability is named electrolocation since it is based on the same principle as echolocation with the electric field replacing the acoustic waves. One of the best studied electric fish in terms of object perception is the Mormyrid *Gnathonemus* *petersii* (see Fig. 1). The active electrolocation of this fish, has a range of one body length [2]. It is based on the emission of a dipole-shaped electric field (see Figure 1) named the carrier, by polarization of the body relative to an emitter-organ in the tail named the Electric Organ of Discharge (or EOD) [3]. The high internal conductivity of the fish's body relative to the surrounding environment focuses the emitted field lines [4], obliging them to flow through its specialized electro-sensitive skin. Discrete electro-receptors distributed all over the epidermis capture an instantaneous 3-dimensional electric image of the near environment [5], comparing the trans-epidermal electric measurements that would be expected in the absence of any obstacles with the sensory image that is actually measured. As a result, electric fish are able to detect, localize and recognize the shape of objects in their vicinity [6, 7]. Moreover, analyzing the influence of the environment on the amplitude and phase modulation of the carrier, the fish can perceive the electric properties of the materials, as their conductivity, and capacity, which appear as "electric colors" [8, 9]. In short, electric fish can perceive any close object electrically contrasted with respect to water. This short range omnidirectional sense is well adapted to navigating complex environments encumbered by many obstacles such as the roots of the trees of flooded tropical forests which are the natural habitat of electric fish. Hence, electric sense could have a narrow but relevant niche in under-water robotics. Furthermore, it could be used as a complementary short range sense for low level reflex navigation, or for some specific task related to the electric properties of the environment, such as seeking a conductive object among insulating obstacles, or avoiding a hot submarine spring (conductivity being dependent of temperature).

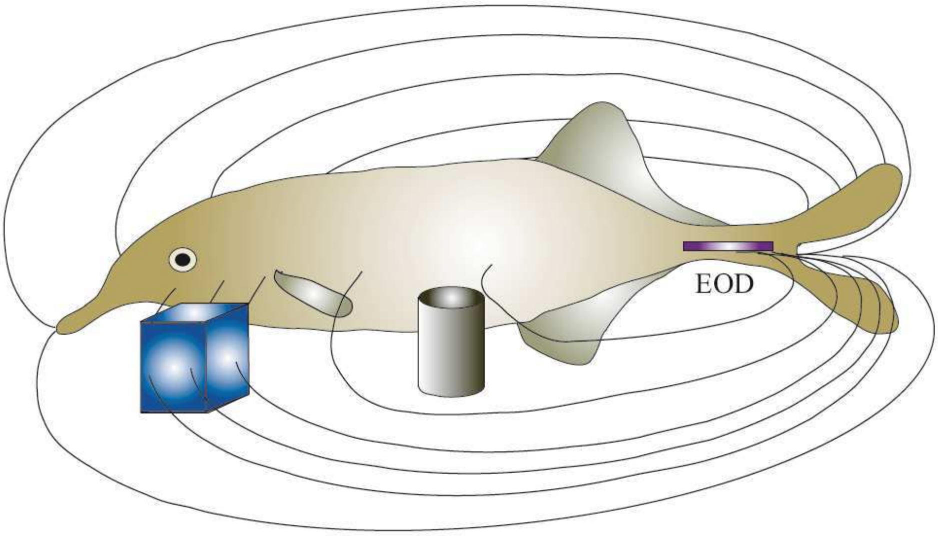

FIGURE 1 – The electric field is distorted by the presence of an object (for instance, an insulating cylinder pushes the field lines away whereas a conductive cube funnels them).

Though potentially interesting, this mode of sensory perception, has been hitherto little studied by engineers [10]. It is only recently that Mc. Iver et Al. [11, 12] have begun to implement the electric sense in robotics. They were the first to construct a detector and its supporting algorithms using only electric sense. Though successful, the proposed approach could not be directly applied to a realistic 3D underwater vehicle since the sensor was only a set of (four) point electrodes with no volume. The measurement mode proposed in [11, 12] can be named U-U mode, the first letter standing for the type of imposed electrical quantity (voltage (U) or currents (I)) and the second for the type of measured electrical quantity (U or I), since a voltage is applied on a first pair of electrodes and measured on the second. The European project Angels [13] is currently developing sensors inspired by electric fish with the objective of implementing the resulting device on a realistic 3D underwater vehicle. The Angels solution offers different working modes differentiated by imposing or measuring current and/or voltage, and can shape the electric field around a vehicle of non negligible volume, using a real-time reconfiguration capability. The purpose of this article is to describe this sensor operating in one particular basic mode, its U-I mode, where a voltage is imposed and the resulting currents are measured. In this preliminary feasibility study, we restrict our investigations to the case of resistive phenomena in laboratory conditions. This allows us to assess the intrinsic capabilities of this new sensor, while postponing the results of its implementation on a real underwater robot to a future article. As we will see, the recovering of the fish range requires a sensor accuracy of 1/1000. Based on basic electronics, the proposed solution achieves a first step towards the implementation of electric sense in robotics.

The article is structured as follows : the second section is devoted to the U-I mode principle, its exploitation for electrolocation and the modeling aspect of the sensor. In the third section we detail the principle of the electrolocation measurement. In the fourth section we show how we adapted our apparatus to the electric properties of tap water. In the fifth section the electronics are fully detailed in relation to the desired task. We then illustrate the test bed in the sixth section. In the seventh section we focus on the experimental results. Special attention is paid to measurement accuracy and its sensitivity to temperature and conductivity. We also present some comparisons between the model and the experiment for specific scenes. Future projects that will use our electrolocation sensor are outlined in section eight. Section nine concludes.

2 The physics of the sensor

2.1 Principle of the measurement

Taking inspiration from the African fishes of the Mormyride family, we designed a device capable of producing a dipolar basal field. In this case, a set of electrodes (named receivers) are put under a controlled voltage with respect to a single ground emitter mimicking the EOD. This creates a current loop around the sensor. Such a current loop polarizes the objects in the surrounding scene which in turn produces perturbations of the measured currents flowing toward the receivers.

2.2 The Modeling of the Electric Perception by a Finite Volume Sensor

Based on the principle stated in the previous subsection, our sensor is a set of groups of metallic electrodes placed on the insulating boundaries of a cylindrical body (Fig. 2). On each group of electrodes, we can impose a potential with respect to a common grounding group playing the role of emitter, while measuring the currents flowing across the individual electrodes.

Our test probes are all based on a common geometry : a cylinder of diameter 20 mm with spherical extremities (see Fig. 2). This slender shape was chosen since it offers the possibility to approximate the electric measurements by simple expansions with respect to the sensor aspect ratio r/L (r is the radius of the cylindrical shape and L is its length). The insulating parts are made of PVC and the electrodes of 316 stainless steel. Several versions have been built with various numbers of groups of electrodes and various segmentations of the electrodes.

As the sensors are slender, we can consider the current emitter and receivers (of ring or hemispherical shape) as an array of effective spherical - electrodes arrayed along a line joining their centers. Such a model is named ”poly-spherical model” in [14]. Furthermore, let us assume that these spherical electrodes are sufficiently distant (with respect to their size) to prevent any

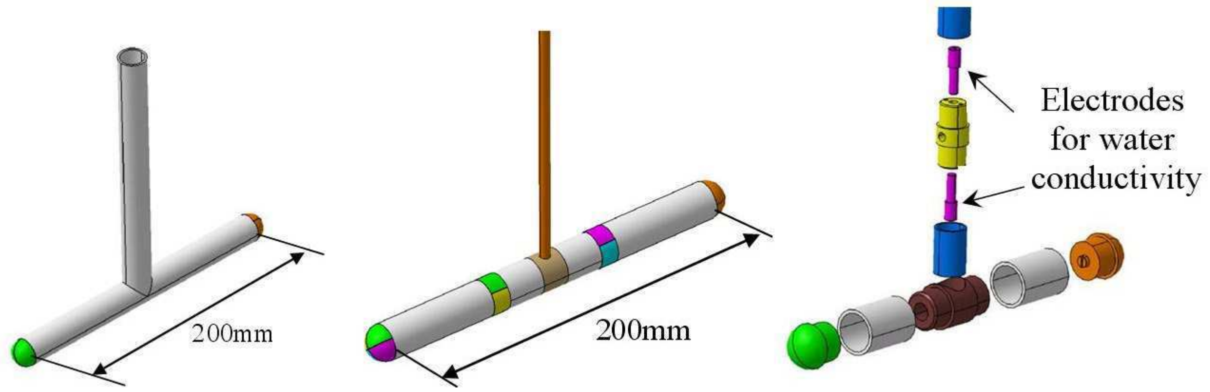

Figure 2 – Electrolocation test probes. Left : Dipolar sensor. Middle : 16-electrode ; each group is composed of four electrodes. Right : Dipolar sensor illustrating mechanical components and the conductivity meter on top of the sensor.

mutual perturbation between them. The vector of voltages U between the emitting electrode and the grounding electrodes (i.e. the current receivers) is linked to the vector of currents I measured on the same electrodes by Ohm's law [14] :

$$I = CU = (C_0 + \delta C)\, U \tag{1}$$

where C and C_0 are respectively the conductance matrix of the external scene with and without object and δC is the perturbation of conductance induced by the presence of an object within the reach of the sensor. Furthermore, we have $C_0 = \gamma S_0$ and $\delta C = \gamma \delta S$ with γ the water conductivity, S_0 a matrix which depends on the sensor geometry only, and δS a matrix depending both on the geometry of the sensor and objects boundaries. This poly-spherical model has been applied to the prediction of the perturbations of large objects such as the insulating walls of a tank in [14], and to small homogeneous objects in [15]. The response of such an object in a quasi-uniform electric field $\mathbf{E}_0$ is chiefly described by the induced dipolar momentum $\mathbf{p}$ [16] whose value is

$$\mathbf{p} = \mathbf{P} \cdot \mathbf{E}_0\,, \tag{2}$$

where $\mathbf{P}$ is the polarizability tensor that encodes the geometry of the object as well as its intrinsic electric properties. Because the model consists of electrodes of spherical geometry it is straightforward to find the associated conductance perturbation δC in the presence of objects of polarizability $\mathbf{P}$:

$$\delta C = C_0 \mathcal{P}^T K \mathcal{P} C_0\,, \tag{3}$$

where $\mathcal{P}$ is a current conservation operator which ensures that the sensor is in electrokinetic equilibrium, i.e. $\sum I_i = 0$. K is a tensor encoding the electric and geometric properties of the object with respect to the sensor :

$$K_{i,j} = -\frac{1}{4\pi\gamma}\frac{\mathbf{r}_i \cdot (\mathbf{P} \cdot \mathbf{r}_j)}{\mid \mathbf{r}_i \mid^3 \mid \mathbf{r}_j \mid^3}\,, \tag{4}$$

where $\mathbf{r}_i$ is the distance vector from the center of the i^{th} (spherical) electrode to the center of charge of the object. Note that the electronics hereafter will propose an in-line measurement of γ which will allow the separation (4) of the influence of water conductivity from that of the boundaries geometry. In particular, S_0 can be evaluated once for all through preliminary measurements of I without obstacles, or calculated with a numerical code capable of modeling arbitrary geometries as the Boundary Elements Method [17, 18, 19].

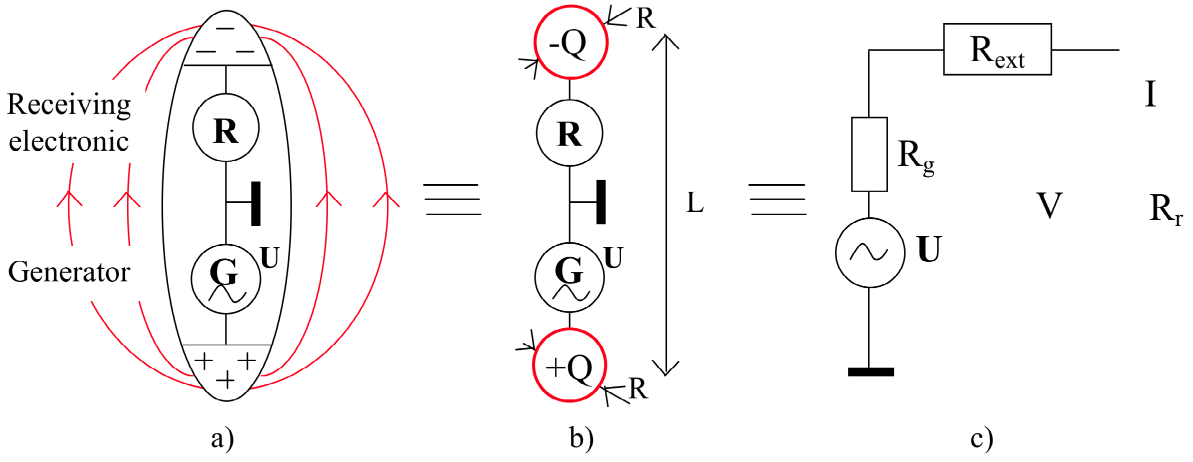

FIGURE 3 – a) The sensor, here composed of two electrodes ; the arrows represent current lines in the external conductive medium and the open circle represents the loading resistance. b) The electromagnetic model. c) The equivalent electric circuit.

The prediction of lateral currents (currents measured in specific sectors of the previously considered electrodes) is out of reach of the poly-spherical model described above and requires a finer modeling, presented in [15] for a cylindrical geometry of the sensor.

3 The Principle of Electrolocation Measurement

3.1 From the Physical Model to the Equivalent Electrical Circuit

To understand the principle of measurement by electrolocation let us start by defining an equivalent electric model of our sensor. For the sake of simplicity, let us focus on a simple slender sensor composed of only two electrodes. This sensor can be considered as two equivalent spherical electrodes of opposite charge $\pm Q$ with a different electrical potential and separated by a distance L sufficiently greater than the radius of the electrodes (see section 2.2 and Fig. 3b). The sensor and its surroundings are equivalent to a simple electric circuit (see Fig. 3c) with an sinusoidale generator U in series with 3 resistances : the internal resistance R_g of the generator, the resistance R_{ext} offered by the external scene to the sensor and the internal resistance R_r of the receiving electronics. Because the internal resistance of the generator and also of the receiving electronics are negligible in comparison with the measured R_{ext} for the U-I mode, the circuit can be simplified by removing the resistances R_g and R_t from the circuit in Fig. 3c. Then the principle of measurement by electrolocation is simply to find an accurate value for R_{ext}. From the theoretical view point, R_{ext} is the inverse of the conductance matrix $C = C_0 + \delta C$ with δC given by (1) in the case of a single object, and which reduces to a single scalar for a sensor with two electrodes.

3.2 Consequences of Current Flowing in Water Medium

One important aspect is the effect of the electrical current on the water. Because tap water is an ionic substance composed of different kinds of elements, chemical reactions can occur when a direct electric current (DC) is imposed [20]. This led us to choose an alternating sinusoidal signal with no DC component. As a result, the principle of electrolocation measurement is the measurement of a signal amplitude modulated by the environment (see Fig. 4).

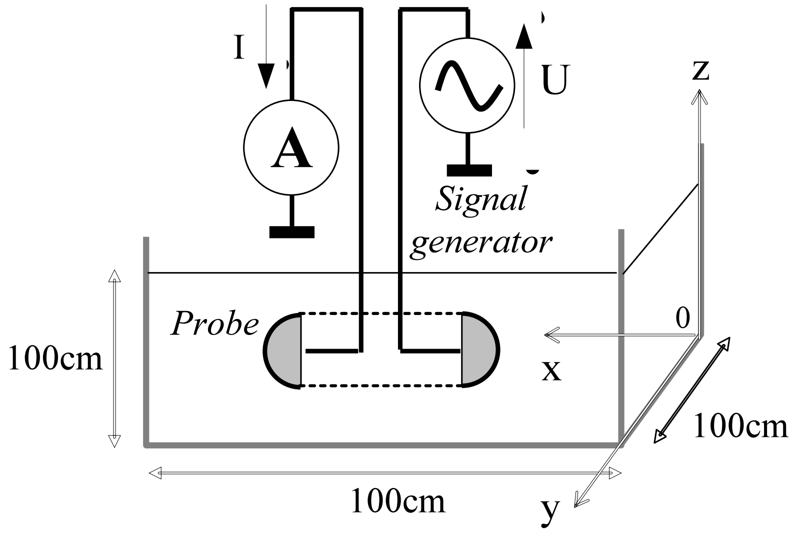

FIGURE 4 – Principle of the measurement : a sinusoidal signal U_0 is imposed to avoid any electrolysis. As a result the electrolocation sensitivity is a modulation of a current or voltage (here a current I) on the electrodes

3.3 Accuracy Requirements

To estimate the accuracy required for detection of large obstacles, let us consider a dipolar sensor like the one depicted in Fig. 2a and 3a submerged in a tank with no object. We can deduce (section II of [14]) an expression of the relative resistance perturbation for a dipolar sensor perpendicularly facing a wall made of material whose conductivity is much lower than the conductivity of water (referred hereafter as an "insulating wall") :

$$\frac{\delta R_{\text{ext}}}{R_{\text{ext}}} = \frac{(r/L)}{4\widetilde{d}(1+\widetilde{d})(1+2\widetilde{d})}\,, \tag{5}$$

where R_{ext} is the resistance with no object, δR_{ext} is the additive resistance induced by the wall, r is the radius of the electrodes, L is the length of the sensor and $\widetilde{d} = d/L$ with d the distance between the front electrode and the wall. This expression (5) is valid provided the polarization on each of the electrodes under the influence of the wall can be neglected. This is indeed the case when the closest distance between the wall and the sensor (d) is much larger than r. Defining an electrolocation distance range of $d = L$ with an electrode radius of $r = 1$ cm and a length $L = 20$ cm, one obtains from eq. (5) that

$$\frac{\delta R_{\text{ext}}}{R_{\text{ext}}} \simeq 0.2\%\,, \tag{6}$$

which corresponds to the minimal sensitivity mandatory to detect the wall at such a distance d. To achieve this accuracy we adopted in this preliminary feasibility study the following methods :

- Use of a band pass filter to eliminate high and low frequency noise.
- Simultaneous measurement of the amplitude of the imposed voltage signal and the measured currents to take into account amplitude variations of the sinusoidal generator device.
- A statistical measurement of 1000 values to estimate a mean value and standard deviation reflecting the quality of the measurement (see section 7.1).

In a further step, the synchronization of emission and reception can be avoided, for instance by using a RMS to DC converter on each of these signals.

4 Adaptation to the Electrical Characteristics of the Probe in Fresh Water

The electrical conductivity γ of a material, defined as the inverse of the resistivity ρ, is obtained experimentally by measuring the resistance R of a volume of section A and length l of this material and then using the following formula :

$$\gamma = \frac{l}{RA}. \tag{7}$$

4.1 Temperature Response of water

Besides the fact that the water conductivity is dependent on the concentration of ions, it is also dependent on temperature and frequency [21, 22]. For our purpose, we will resort to the following simplified formula as for the temperature dependence :

$$\gamma_{_{\mathbf{T'}}} = \frac{\gamma_{_{\mathbf{T}}}}{1 + \beta\,(T - T')} \text{ with } \beta = \frac{1}{\gamma}\frac{\partial \gamma}{\partial T} \simeq 1 \text{ to } 3\% \text{ per } {}^\circ\text{C},$$

where $\gamma_{_{\mathbf{T'}}}$ (resp. $\gamma_{_{\mathbf{T}}}$) is the conductivity at temperature T' (resp. T) and β is the temperature compensation slope of the material. Conductivity measurements carried out on the water supply in our laboratory showed a dispersion at constant temperature (25°C) that ranged from 360 μS/cm to 410 μS/cm. This dispersion is due to changes in chemical composition. The measurements of conductivity as a function of temperature are presented in Fig. 5. They were obtained using a conductivity meter WTW Cond 197i. The curve of the temperature compensation slope shows discontinuities related to the low resolution of our conductivity meter (± 1 μS/cm). However the average value appears clearly to be about $\beta = 2.5\%$ per °C, which experimentally confirms the dependence of the conductivity on the temperature of the water. **Note that in order to offer a measurement of conductivity independent of temperature, conductivity meter manufacturers offer to extrapolate the measurement to a reference temperature [1]. The temperature compensation of the conductivity is either linear or non-linear under the standard NE 27888. For our work, we have switched this feature off.**

4.2 Frequency Response of Water

The electrical signals emitted by fish for electrolocation are of two distinct types : sinusoidal signals (in all *Gymnotiforms* except *Gymnotus carapo* and *Electrophorus electricus*) and pulse signals (in the *Mormyridae*). Fishes belonging to the same species do not generate both types of signals. In order to simplify the specifications of the signal processing electronics (amplifier, current / voltage, filter, etc.), our preliminary study of the electrical sense has been focused on the sinusoidal voltage type. To understand the electrical behavior of our laboratory's water supply coupled to the sensor, we measured the complex impedance Z of a dipolar hemispherical probe electrode immersed in several tanks of volume equal to 25 l (small tank), 150 l (medium) and 1000 l which corresponds to the (large) tank where experiments are carried out (see Fig. 4). All these tanks (small, medium and large) are filled with tap water of conductivity γ equal to 0.0432 S/m, 0.0406 S/m and 0.0432 S/m respectively. In all cases, the results presented in Fig. 6 can be qualitatively understood as the combination of three dominant features : a) the presence of a shallow minimum for the capacitance of water for frequencies between 5×10^3 Hz and 5×10^4 Hz, well established in literature [23], b) an increase in the contact impedance

---

[1] In the case of WTW Cond 197i conductivity meter, two reference temperatures 20 °C or 25 °C are available

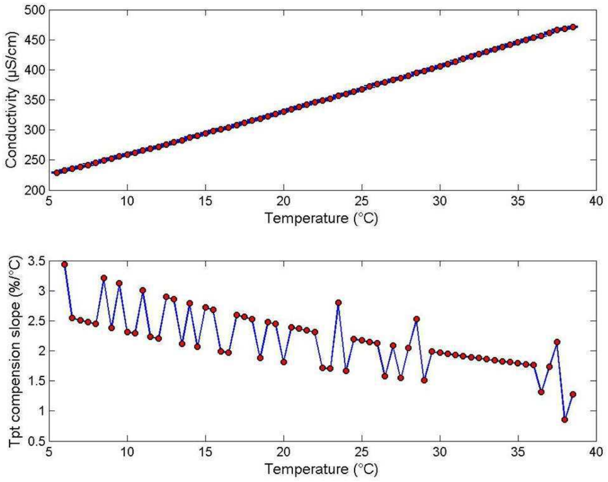

Figure 5 – Top : water conductivity versus temperature ; bottom : temperature compensation slope versus temperature

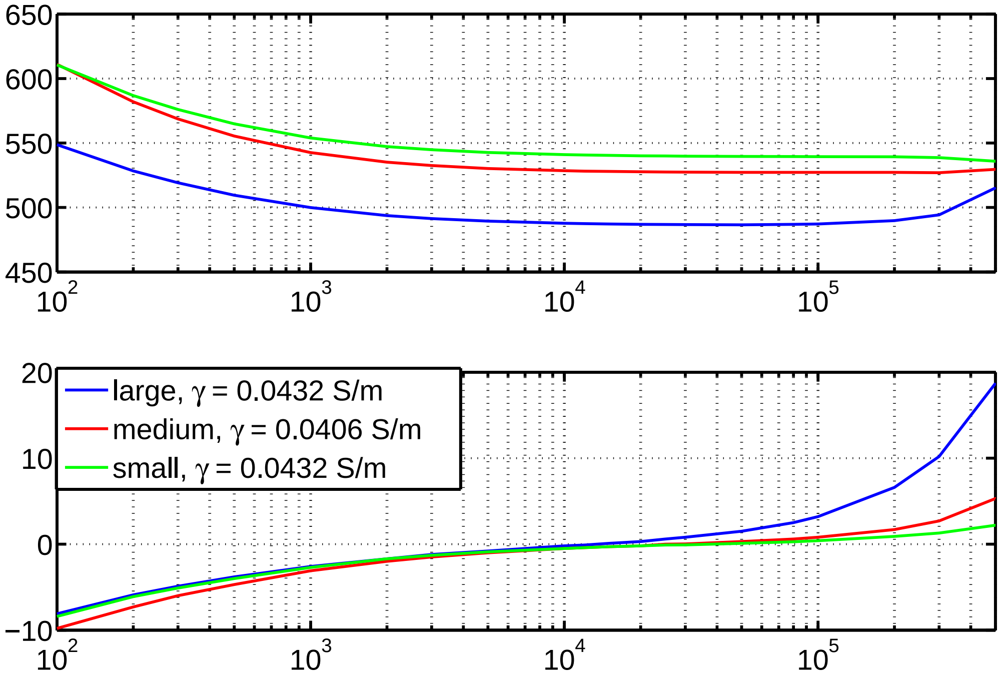

Figure 6 – Complex impedance of our dipolar probe immersed in a 220-liter tank of water.

between the electrodes and the water at low frequencies ($\nu \lesssim 10^3$ Hz), in particular its capacitive component [24], and c) the impedance of the coaxial cable, that manifests itself mostly at high frequencies ($\nu \gtrsim 10^5$ Hz). Finally, in the band where the capacitance gets its minimum value, Z can be approximated by a pure resistive component. This feature being observed on any of the tanks, it is independent (probably beyond a certain minimum value) of the size of the tank. Thus, to be in agreement with the resistive model of the article (section II.B), the frequency chosen for our study in sinusoidal operating mode is in the intermediate band 5×10^3 Hz $\lesssim \nu \lesssim 5 \times 10^4$ Hz (see Fig. 6) where the immersed probe can be considered to be purely resistive.

5 The Electronics

5.1 Basic principle

In a general way, we can define an electrolocation sensor as a set of N electrodes attached to an insulating body. To open the field of study as widely as possible, Angels is developing a sensor on which one can either, for each electrode, impose the voltage and measure the current or impose the current (possibly 0 in passive measurement mode) and measure the voltage. However, this article focuses on the particular case where voltages are set and current measured. Our first electronic prototype based on this principle has been achieved. A simplified configuration of the overall configuration corresponds to a sensor in which all electrodes measure currents (I_k) and are set to the same voltage (virtual ground), except one distinguished electrode which is set to an imposed voltage U_1 (see Fig. 7). This electrode is located in one tip of the prob like the EOD of the fish is in its tail.

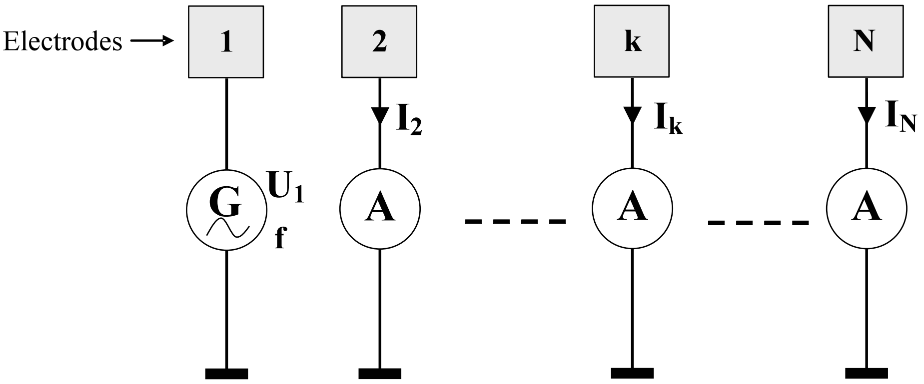

FIGURE 7 – Electrolocation sensors in $U-I$ mode. Here the electrode 1 is the current emitter

5.2 Signal Generator

The final aim of our research project is to design on-board sensors for autonomous underwater vehicles (see section 8). However in this preliminary feasibility study, we used an external sinusoidal signal generator. In this remote configuration, a laboratory Low Frequency Generator is coupled to an operational amplifier mounted in follower mode. The frequency of the sine wave is $f = 22.5$ kHz. For the embedded generator, an integrated circuit function generator EXAR XR2206 has been chosen. A prototype circuit has been built and tested (see Fig. 8). The sinusoidal signal generation is validated and the circuit is implemented on the Angels multi-electrode sensor.

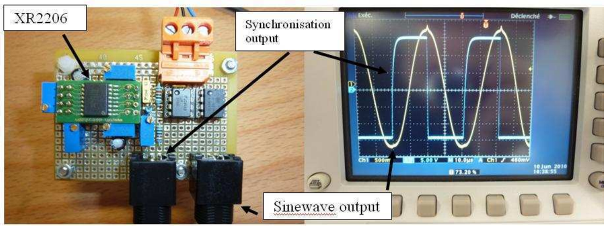

FIGURE 8 – Prototype circuit of embedded generator and test result.

5.3 Receiving Electronics

The receiving electronics are illustrated in Fig. 9. One analogue channel consists of a current-voltage amplifier associated with a second order band pass filter. The measuring electrodes are connected to the current input of the preamplifier which is a virtual ground (see section V.A). We name $R_{\text{ext},1-k}$ the external resistance of the scene between the electrode imposing voltage 1 and the measuring electrode nk. In the case of the external signal generator, the cables transmitting the electrical signal to the electrodes are relatively long (5 m) and we had to take their resistances r_1 and r_k into account in the theoretical study (see Fig. 9). The resonant frequency of the filter device (Rauch) was chosen so as to equal the frequency of the sine wave. In these conditions, the transfer function of the filter is equal to $T_{\text{filter}} = -\frac{1}{2}$, and the dependence between the voltage generator V_{IN} and the filter output V_{OUT} is given by :

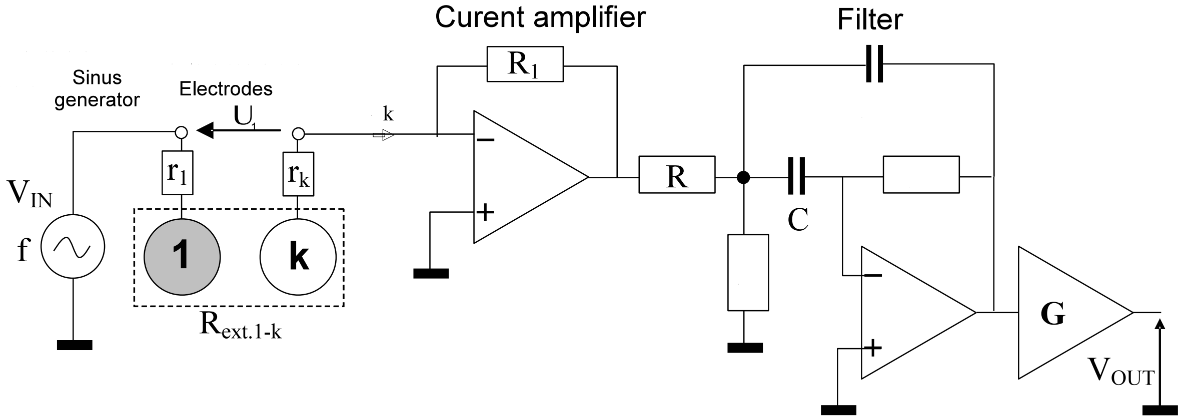

FIGURE 9 – Schematic of receiving electronic in $U - I$ mode (1 channel).

$$T = \frac{V_{\text{OUT}}}{V_{\text{IN}}} = \frac{GR_1}{2(R_{\text{ext},1-k} + r_1 + r_k)}\,, \tag{8}$$

where G is the output gain of the filter. We express the external resistance of the scene as a linear function of the voltage ratio $V_{\text{IN}}/V_{\text{OUT}}$. These voltage amplitudes are acquired experimentally by an analogue to digital converter triggered to perform the conversion at the maximum and at the minimum of the sensed signal, assuming the environment is purely resistive. In these conditions, one can measure the external resistances through :

$$R_{\text{ext},1-k} = A\frac{V_{\text{IN}}}{V_{\text{OUT}}} + B, \text{ with } A = \frac{GR_1}{2};\ B = -r_1 - r_k\,. \tag{9}$$

Due to the fact that the measuring electrode is at potential zero, the application of Ohm's law allows one to find that the current flowing toward the electrode k is given by :

$$I_k = 2\frac{V_{\text{OUT}}}{GR_1}\,. \tag{10}$$

Fig. 10 shows an 8-channel 4-layer PCB implementation of the receiving electronics.

To achieve a measurement of good accuracy, the coefficients A and B are obtained by way of calibration. This calibration consists in connecting a set of standard resistors of R_{cal} (tolerance : ±0.01%) with a low temperature coefficient (TCR : ±0.6ppm/°C) to the receiving electronic input. For each of these standard resistors, a population of 10000 measurements is acquired for

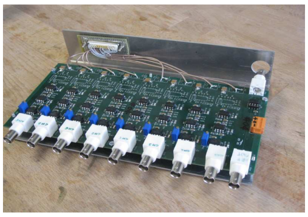

Figure 10 – Receiving electronics in $U-I$ mode (8 channels).

statistical study[2]. A linear regression using the least squares values is applied to the average values of each population to determine the coefficients A and B. Fig. 11 shows a calibration curve for one channel. The displayed residuals are less than 0.01% in magnitude and well scattered around zero, indicating the absence of any significant non-linear component. When the tolerance of calibration resistors is combined with the amplitude of the regression residuals, a minimal accuracy of our measurement device of about ±0.02% is deduced. This accuracy is compatible with the expected one of section 3.3.

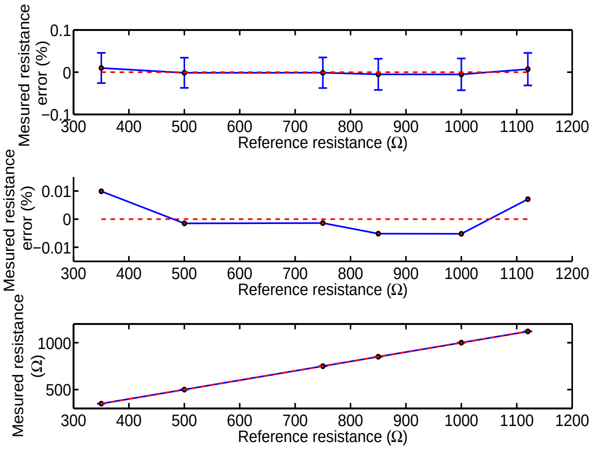

Figure 11 – Calibration of one channel of the receiving electronics ($A = 2457.8\Omega$, $B = -5.9169\Omega$). The error bars represent ± the standard deviation of a population of 10000 measurements.

With several measuring electrodes, the same method can be applied in order to determine the currents flowing toward each of the receivers, except that $R_{\text{ext},(1)-k}$ is not the external resistance of the scene but the inverse of $C_{1,k}$, where C is the conductance matrix described in section 2.2, and all $(R_{\text{ext},1-k}) + r_k$ branches are connected in parallel to the emitting electrode.

6 The Experimental Bench

6.1 Tank and Robot

In order to test our electrolocation sensors in controlled and repeatable conditions, an automated test bench consisting of a one cubic meter tank and a three-axis Cartesian robot, has been built (see Fig. 12). This gantry was fixed on the top of the tank and allowed the probe to be

---

[2] with a resulting standard deviation of 0.02% – see section 7.1 as well – which indicates that the statistical error performed on each average is $\approx \frac{0.02\%}{\sqrt{10000}}$ and thus negligible with respect to the intrinsic tolerance of the calibration resistors

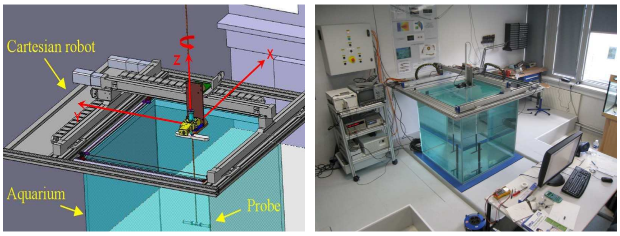

(a) $3D$ modeling (b) experimental set-up

FIGURE 12 – Electrolocation test bench.

positioned in translation along its X and Y axes with a precision of 1/10 mm. The orientation in the horizontal plane was adjusted to absolute precision of 0.023 ° using an absolute rotation stage (see Fig. 13). All probes tested were positioned in the tank using a rigid glass epoxy fiber tube (∅14 mm) whose height is adjustable. This isolating tube allows the passage of electrical cables dedicated to the signals coming from the electrodes to readout electronics (analogue chain + ADC board) without compromising the measurements. Its vertical orientation is ensured using a micrometric adjustment base. Our test also allows dynamic trajectory management at a significant range of speeds relative to the tank size. The maximum speed available was 300 mm/s ($\simeq$ 1 km/h) for both translations and 80 °/s (13.5 rot/min) for rotation.

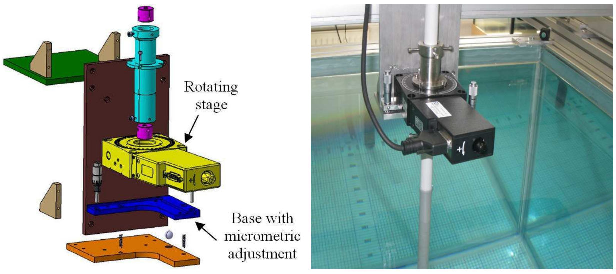

(a) CAD (b) experimental set-up

FIGURE 13 – Stage-keeping probe.

This test-bed allows one to separate the problem of underwater locomotion (of our future robots) from that of the perception, and to study the intrinsic capabilities of the electric sense before its implementation on a real autonomous robot.

6.2 Computer Monitoring of the Robot

We chose a three axes robot computer control using simulink software with the dSpace system. The entire structure of the system is given in Fig. 14.

The electrolocation signals coming from the electrodes of the probe are first processed by analogue chain (amplification and filtering), then converted by a 16-bit ADC, DS2004 card with a resolution of 0.3 mV/bit to 0.15 mV/bit (range from ±5 V to ±10 V). This card allows us to convert all 16 channels at the same time at a maximum speed of 1.25 MHz.

6.3 The Objects

To test the measurability of objects of simple geometry using electric sense, a set of test objects were fabricated with conductive and insulating materials (see Figures 15 and 16). We fabricated objects of similar density to water in order to be able to keep them under water

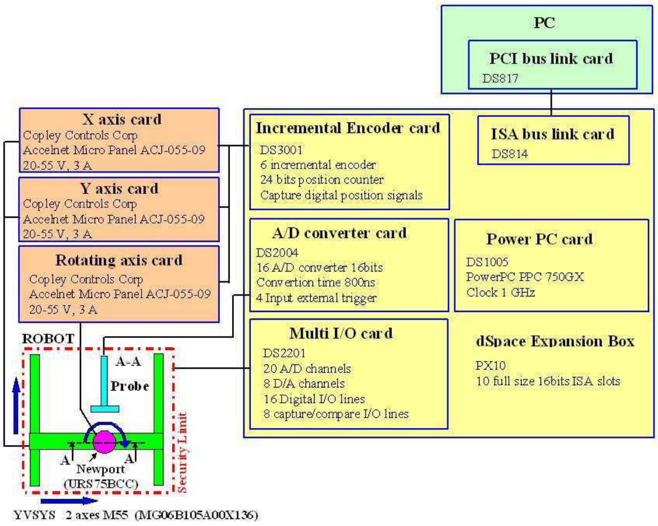

Figure 14 – Computer monitoring of the test bench.

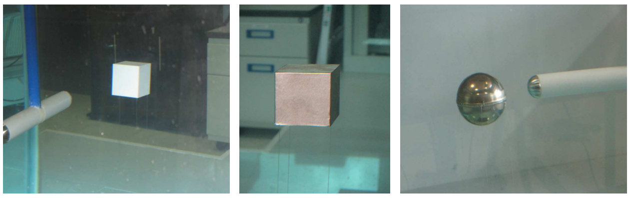
(a) (b) (c)

Figure 15 – Test objects : a)insulator cube (side= 40 mm), b) conductive cube (side= 40 mm), c) conductive sphere ($\oslash = 40$ mm)

easily when using weakly invasive bonds such as nylon filaments or non-conductive rods of small diameter (1 mm) (see Fig. 16).


(a) mounting of a conductive ellipsoid (b) ellipsoid set (conductive and insulating) (c) mounted conductive ellipsoid

Figure 16 – Ellipsoid object.

7 Experimental Results

7.1 Characterization of Electronic Noise of the experimental test bed

A characterization of the total noise of the analogue electronic chain has been performed. The Fig. 17 shows the experimental set-up.

Two types of external resistor R_{ext} were connected to our electronic device in order to characterize the level of noise in the conditions of our experiments. The first type are the standard

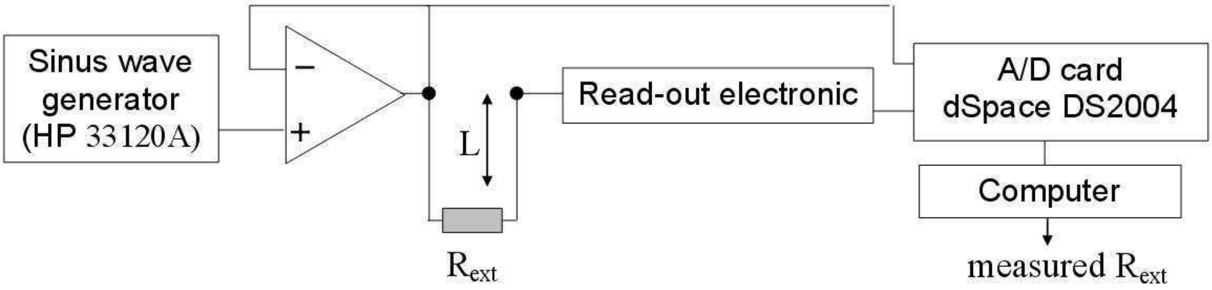

FIGURE 17 – Schematic of experimental set-up for measuring noise

resistors already used for the calibration process (see section V.C) whose resistance is known accurately, while the second type is the probe itself, immersed in the tank filled with tap water and placed in radial contact to the wall at the level of its center with the motors of the gantry first switched on and then switched off.

On Fig. 18a we represent the distribution of $N = 10000$ measurements, that is to say N successive single ADC conversions, each of them lasting 15 ms. One observes an average value located at 0.04 Ω from the expected value $R_{\text{cal}} = 500$ Ω given by the manufacturer (i.e. relative error 0.008%). This is compatible with an intrinsic accuracy for R_{cal} of 0.01%. Thus, 0.02% defines the precision of the sensor, which is compatible with the requirements of section 3.3. This noise could have several origins such as filtering defects or amplitude fluctuations in the power supply, or electromagnetic compatibility issues between the various electronic components or even between the electronic boards [25, 26]. The electronics components themselves could even be responsible for this noise, as the chosen electronics are not of "low noise" type.

For the second characterization, the cable length from the probe to the electronics was $L = 5$ m. With motors switched off (see Fig. 18b), the distribution of the measurements shows a Gaussian noise, which is fairly similar to that of the standard resistor. This shows that both the extra cable and the water environment are low sources of noise compared with the electronics. When the motors of the gantry are switched on (see Fig. 18c), the distribution of the measurements, highlights a non-Gaussian noise, which is explained by the fact that the motor supply generates non-random noise. We note that some measurements seem very distant from the average value (some 10 Ω). The width at half height of this distribution is 0.7 Ω, that is 1.9 times higher than that obtained for the standard resistor. From these characterizations we conclude that the dominant sources of noise are the electronics and the motors of the gantry.

7.2 Drift Test in Temperature of Electronics

We have already presented an experimental measurement dispersion of ±0.02% (see sect. 5.3) at room temperature. As such a small value is required in order to detect objects of low electrical disturbance, we have assessed its stability with respect to other physical parameters. Temperature is a significant factor in measurement stability, therefore the receiving electronics were tested at various temperatures. For this purpose, the circuit was placed in a stove with a standard input resistor 500 Ω ± 0.6 ppm/°C located outside.

The outside temperature was 20 °C ± 1°C throughout all the duration of the experiment, implying a negligible drift of the resistor value (±0.3 mΩ). The measurements have been considered only after stabilization reflecting the uniformity of temperature in the stove. By restricting the temperature maximal value to 55 °C, the results of this test show a resistance deviation of the order of ±0.005%, as illustrated in Fig. 19. As this value is well below the required accuracy of ±0.02% we conclude that our electronics is robust enough against temperature fluctuations and necessitates no temperature correction.

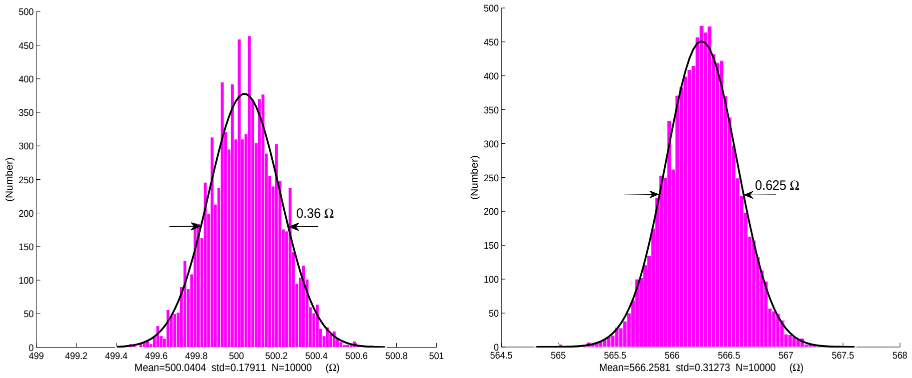

(a) standard resistor $R_{\text{cal}} = 500\ \Omega$ (motors off)

(b) probe resistance in water with motors off

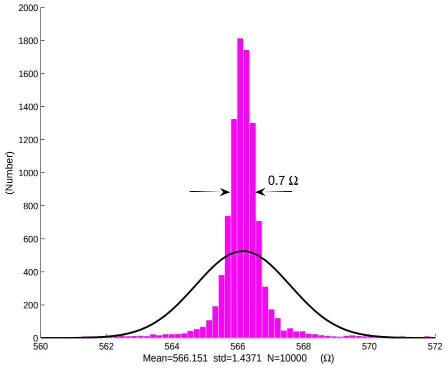

(c) probe resistance in water with motors on

FIGURE 18 – Histogram : distribution of resistance measurements obtained with $U-I$ electronics for a population of $N = 10000$ individual measurements ; plain line : “best” gaussian fit, of same average and standard deviation as the distribution.

7.3 Measurements with Test Probes

7.3.1 Wall detection

The first electrolocation results were obtained using the probe with two electrodes described in section 2.2. This probe has a cylindrical geometry of $2r = 20$ mm and an overall length of $L = 220$ mm. It consists of two stainless steel hemispherical electrodes separated by an insulating tube made of PVC. The gantry was programmed to move the probe from one wall of the tank to the other in the X-axis while the probe remained centrally placed with respect to the Y- and Z-axes throughout. The walls are made of glass and are considered as pure insulators as they have very low conductivity relative to tap water. The dimensions of the water surrounding the probe are 971.5 mm × 971.5 mm × 975 mm and the conductivity measured is 356 $\mu S/\text{cm}$ (typical value). The walls are nicely detected by a significant increase of the resistance, i.e. a significant decrease of the measured current (see Fig. 20) as the probe approaches the wall.

For a probe starting in the center of the tank ($X = 0$), a natural way to set a limit of detectability (or range) is to require that $R_{\text{ext}}(X) = (1 + 0.02\%)\, R_{\text{ext}}(X = 0)$, where 0.02% corresponds to the precision of our device. This leads to $X \approx 110$ mm, that is a distance between the wall and the front electrode of $d = 266$ mm ≈ 1.2 times the probe length ($d \approx 1.2L$).

This first study shows that the electrical sense is a moderate-range mode of perception for large objects like walls. More precisely, the wall was detected at a distance of about one probe

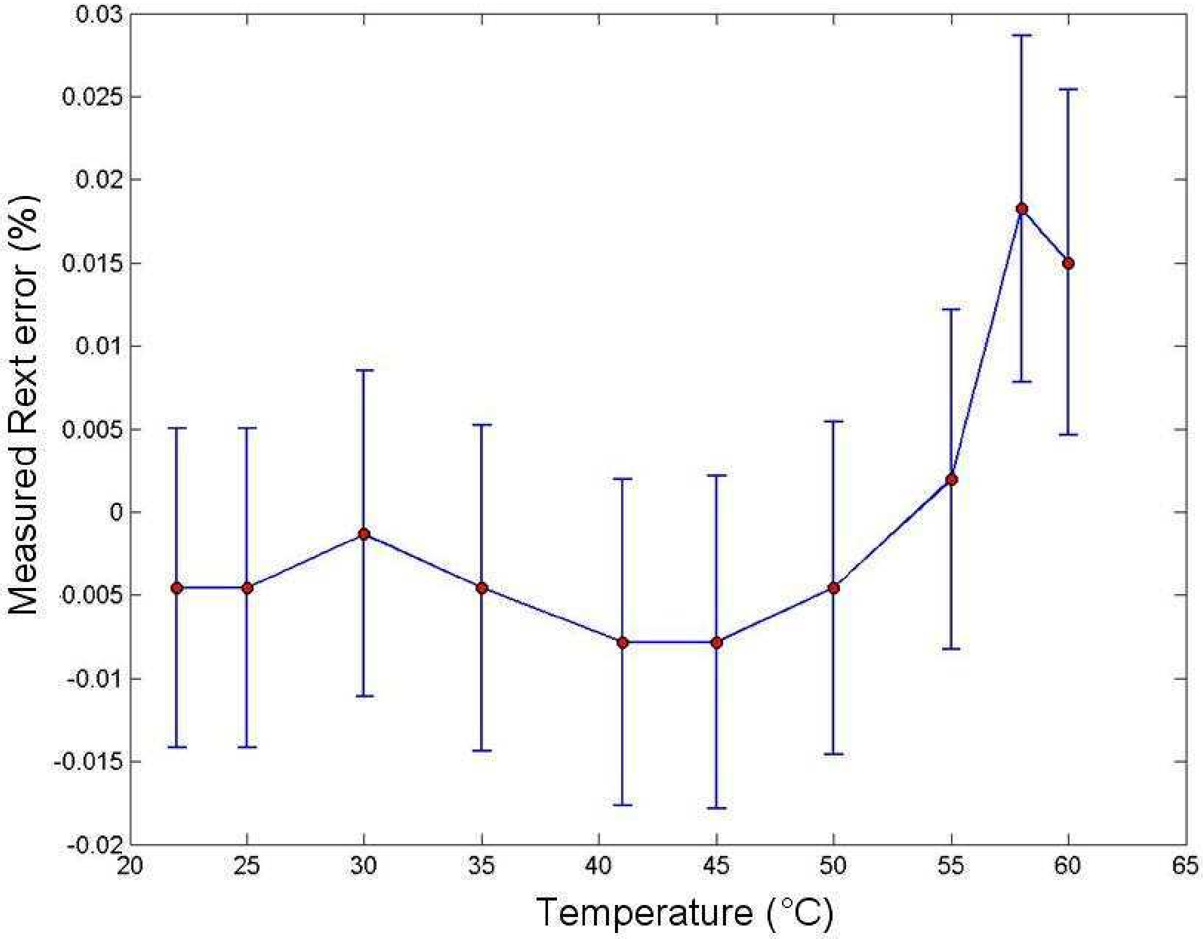

FIGURE 19 – Temperature drift of the U-I receiving electronics ; the error bars represent the standard deviation obtained with a population of 1000 measurements for each temperature.

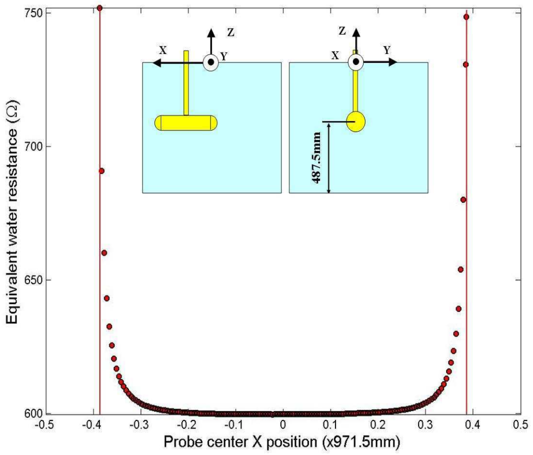

FIGURE 20 – External resistance measurements for a wall to wall crossing of the sensor.

length, which is similar to the range of active electric sense of fish.

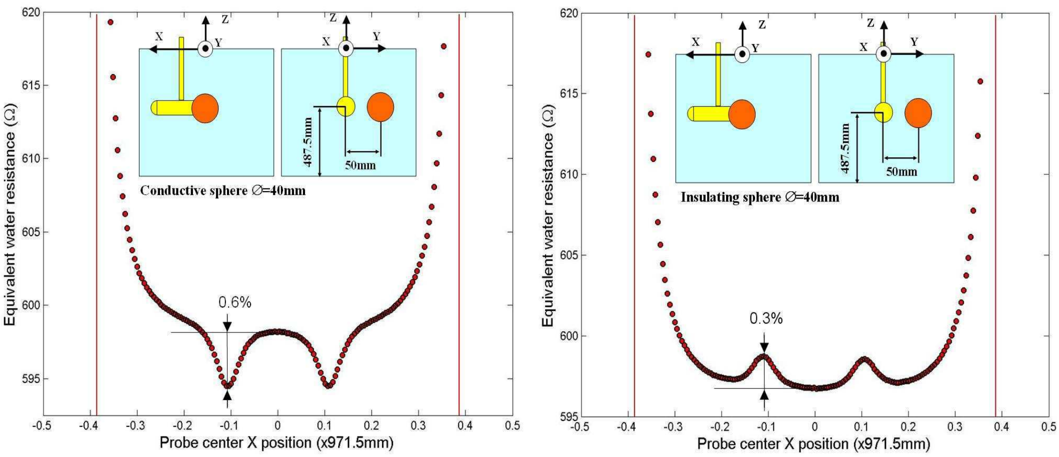

(a) conductive sphere

(b) insulating sphere

Figure 21 – External resistance measurements for a wall to wall crossing with 40 mm spherical object placed at 50 mm. a) Water conductivity $\gamma = 356$ μS/cm. b) Water conductivity $\gamma = 359$ μS/cm.

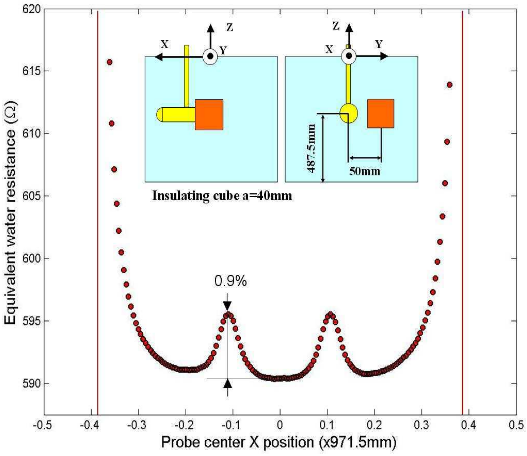

(a) conductive cube

Figure 22 – External resistance measurements for a wall to wall crossing with a cubic object ($a = 40$ mm placed at 50 mm). Water conductivity $\gamma = 359$ μS/cm.

7.3.2 Object detection

To show the sensitivity of our electrolocation device to the presence of objects of different conductive types and shapes, we present in Figures 21 and 22 the external resistance measurements for a probe, an electronic device and a trajectory unchanged with respect to those of the previous subsection (a tank with no objects).

Four objects were used. One was a conductive cube of side = 40 mm. Two were spheres ($\emptyset = 40$ mm), one insulating ; one conductive.

Passing next to the objects, the resistance measurement increases if the object is insulating and decreases if the object is conductive (see Figures 21 and 22). Two peaks appear during the movement, which correspond to the positions of the objects at the minimal distance from one of the two electrodes. Analysis of the curves in Figures 21 and 22 shows that the conductive nature of the objects is easily identifiable by observing the increase or the decrease of the external resistance as the probe passes close to the objects. Despite the small distance between the probe center and the object center (50 mm), their presence results in a visibility average which remains low, ranging from 0.3% to 0.9%. The measurements taken under the same conditions as above (Fig. 22a) but for an object distance of 100 mm from the probe reveals visibility even lower at 0.03% which is one order of magnitude lower than for a 50 mm distance (see Fig. 23). In addition one can also observe the sensitivity of the method for the shape of the object. We recover the fact that for a same object geometry, the influence of a conductive material is two times higher than for an insulating material while for a same material, the measurement is proportional to the object volume at the leading order [6]. As a consequence, in the case of the cube, since its volume includes that of the sphere, the measurement peak of Fig. 22 is higher than that of the sphere (Fig. 21).

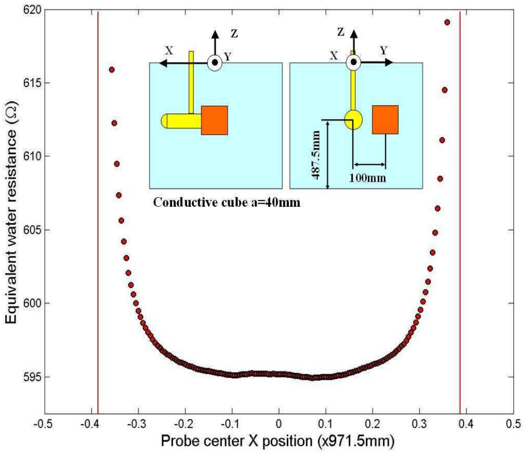

Figure 23 – External resistance measurement for a wall to wall crossing with cubic object $a = 40$ mm placed at 100 mm.

This study has demonstrated the ability of a two electrodes sensor to detect small size objects relative to its length. Their conductive difference was easily highlighted. However, it is confirmed that the electric sense is of short range for this case (between one-third and one half of the total length). Furthermore, the response of each of the sensor's electrodes is maximum when the object faces it while it rapidly decreases when the object moves away along the sensor. A natural consequence of this feature is that the two-electrode sensor loses contact with the object when it is located between the electrodes. This induces a small blind-spot in the detection, visible between the two peaks in Figs 21 and 22. This drawback can be overcome by adding more electrodes to the design. On Fig. 24, we show the currents for the 4-electrode sensor of Fig 2b passing by a conductive cubic object in the same conditions as in Fig. 22. As the sensor moves forward, the conductive cube first faces the head receiver electrode ($X \simeq -0.1$ m), whose external resistance is hence lowered; next ($X \simeq -0.03$ m), the cube faces the body electrode closest to the head, whose external resistance is in turn reduced. For $X \simeq 0.1$ m, the cube faces the emitting tail electrode with an overall decrease of all equivalent resistances. For the body electrode located closest to the tail, we do not observe a doubly-peaked structure but a single minimum for $X \simeq -0.07$ m. In conclusion, one observes a good mapping between the object position along the sensor and the ordering of the current peaks for the various electrodes which allows the contact with the object to be maintained.

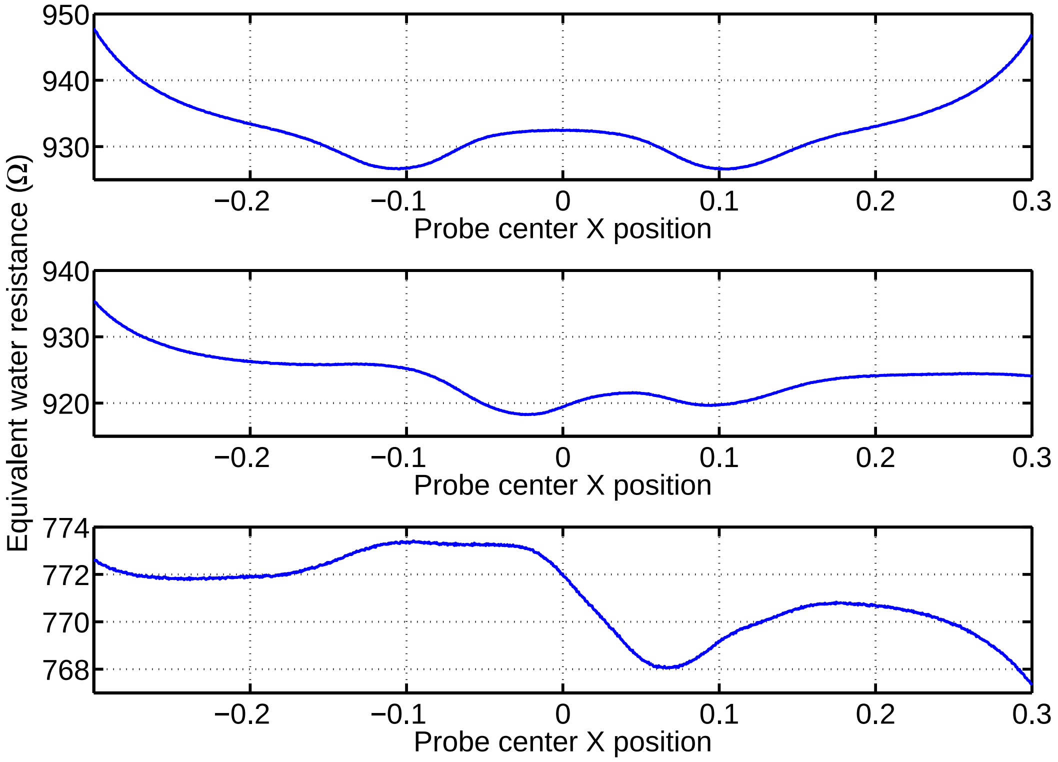

Figure 24 – External resistance measurements by a 4-electrodes sensor for a wall to wall crossing with a conductive cubic object $a = 40$ mm placed at 50 mm. Top, middle and bottom panel correspond to the resistance measured respectively by the "head" electrode, by the body electrode located closest to the head, and by the body electrode located closest to the tail.

7.4 Influence of water Conductivity

The external resistance offered by the environment R_{ext} is inversely proportional to the conductivity γ. The changes in these two quantities are related as follows :

$$\frac{\Delta R_{\text{ext}}}{R_{\text{ext}}} = -\frac{\Delta\gamma}{\gamma}. \tag{11}$$

Conductivity variations related to the chemical composition of water can be controlled throughout the experiment by avoiding external contamination. The conductivity is also strongly dependent on the temperature, so that the external resistance varies as a function of temperature as follows :

$$\frac{1}{R_{\text{ext}}}\frac{\partial R_{\text{ext}}}{\partial T} = -\frac{1}{\gamma}\frac{\partial \gamma}{\partial T} = -\beta\,, \tag{12}$$

where β (=1 to 3%/°C) is the temperature compensation slope of the water and T is the temperature. We have shown the experimental influence of temperature on the external resistance by placing the probe motionless in the middle of the 1 m^3 aquarium and performing measurements over time thus allowing for natural daily variations of temperature. Despite the large volume of water, the relative deviation of resistance reaches 0.2% ($\Delta R_{\text{ext}} = 1\ \Omega$) in 5000 s (see Fig. 25), that means, for a temperature compensation slope of 2.5%/°C, a cooling of about 0.08 °C.

Another experiment showed the influence of temperature on external resistance measurement. The probe crossed the tank and returned at low speed (see Fig. 26). In the middle of

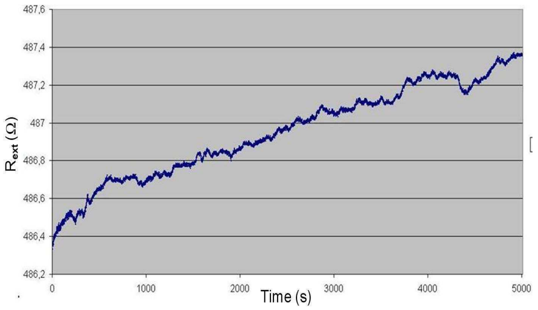

FIGURE 25 – External resistance versus time due to natural convection cooling of the 1 m^3 tank.

the tank, the curve below shows that the relative deviation of resistance between the outward and return travels is 0.06% ($\Delta R_{\text{ext}} = -0.3\ \Omega$). For a temperature compensation slope of about 2.5%/°C, we deduce an increase of the water temperature of about 0.025 °C. Note that such a resistance deviation of 0.06% cannot be attributed to the temperature drift of the electronics since it stood at 0.005% (which is an order of magnitude lower) for a larger range [22 – 55 °C]. To express the impact of this low temperature increase in terms of positioning accuracy, let us consider the positions X_{ret} for which the resistance on the return crossing admits the same value as the one for $X_{\text{for}} = 0$ (corresponding to the aquarium center) on the forward travel. The absolute difference $|X_{\text{ret}} - X_{\text{for}}|$ quantifies the lack of repeatability due to temperature increase and is found to be of the order of 150 mm (see Fig. 26), which is unacceptable.

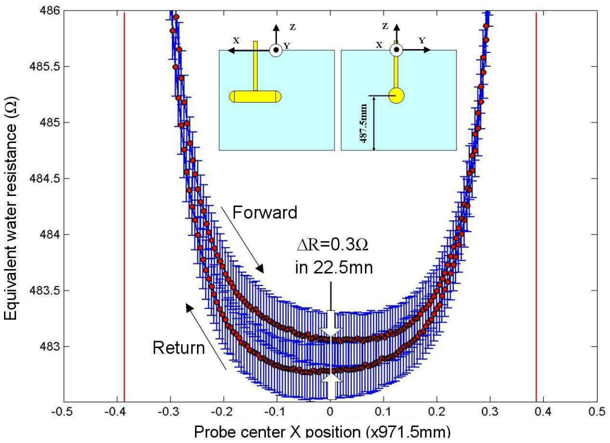

FIGURE 26 – Influence of temperature during a forward and return crossing of the probe.

7.5 Correcting for water Conductivity Variation

The problem of the influence of variations in water conductivity on the electric measurements can be solved by directly measuring γ. In this perspective, an independent conductivity sensor will be implemented on the various prototypes of electrolocation (probes and robots). It will be similar to the electrolocation sensor, but much smaller and hidden in a dead zone of the sensor (robot) boundaries in order to be indifferent to the variations of the external environment geometry. Assuming a uniform conductivity of the water around the sensor, the resistance R_{cond} provided by this independent conductivity meter can be used to normalize the external resistance offered by the scene $R_{ext} = (\gamma S)^{-1}$ (with $S = S_0 + \delta S$ defined in section II.A), according to the formula :

$$R_{\text{ext},N} = \frac{R_{\text{cond},0}}{R_{\text{cond}}} R_{ext} = \frac{1}{\gamma_0} S^{-1}, \tag{13}$$

where $R_{\text{cond},0}$ and γ_0 correspond respectively to known reference values for the resistance and conductivity of water. To test the feasibility of this conductivity correction, we have built a bi-electrode probe with a conductivity measuring module (see Fig. 27). This module attached to the fiber-glass tube of the probe consists of two cylindrical electrodes containing a space that is continuous with exterior through two holes of $\oslash = 4$ mm. These openings were oriented in the direction of the probe movement to facilitate the renewal of water and to obtain realistic conductivity measurements.

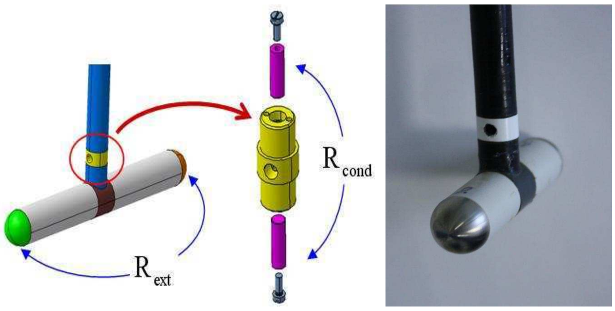

(a) probe structure (b) achievement

FIGURE 27 – Bi-electrode probe with conductivity correction cell.

The experimental results were achieved by modifying the water conductivity (varying the temperature). The curves in Fig. 28 show uncorrected external resistance measurements and corrected values (normalized) for the ambient conditions of temperature and pressure (1 atm, 20 °C). To demonstrate the sensitivity of the corrected conductivity to the external environment, an object was placed in contact beside the motionless probe on the temperature range 5 – 24 °C. The corrected measurements appear to be independent of the temperature or conductivity variation. The presence of an object is detected, which clearly demonstrates that the correction prevents the probe from losing its electrolocation ability.

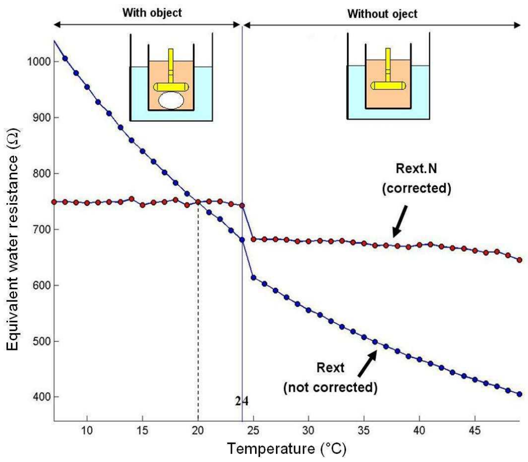

FIGURE 28 – Correction of water conductivity (see text for details).

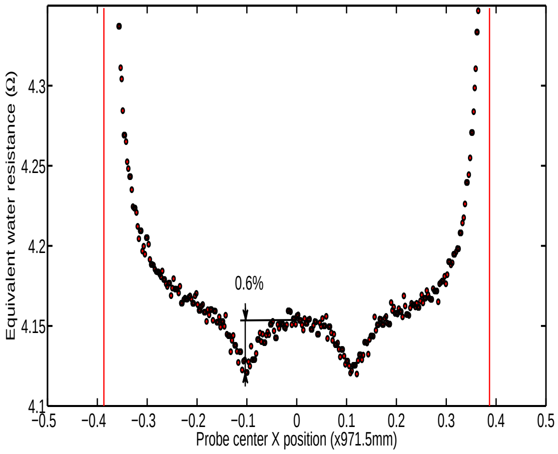

FIGURE 29 – External resistance measurements for a wall to wall crossing with 40 mm spherical object placed at 50 mm in sea water (conductivity $\gamma = 52.4$mS/cm).

7.6 Influence of the salinity of the water

Regarding future application to underwater robotics, the influence of the salinity of on the measurement has also to be studied. In this perspective, we have performed first experimental tests in order to assess the influence of the salinity of water on the sensor performance. First, let us remark that for a given geometry of the scene, and in a range of frequencies where the immersed probe has a pure resistive behavior (see section IV.B), γ does not influence the topology of current lines around the sensor, since it only appears as a prefactor γ^{-1} in the expression of R_{ext} (see (4)), whatever kind of contrasted objects are present in the system. For this reason, patterns observed in Figs. 20 to 24 are preserved, even if the magnitude of R_{ext} diminishes with greater salinity. This, is illustrated on the Figure 29 obtained in the same conditions as those of Figure 21.a but with a water 150 hundred times more salty (i.e. water conductivity is shifted from 356μS/cm to 52.4mS/cm, which corresponds to the conductivity of sea water). On this plot, we recover the same response as that of Figure 21.a, but shifted of two orders of magnitude. This has been obtained by shifting the generator frequency f from 25.5 to 17.5 kHz and by re-calibrating A and B in (9) with a set of standard resistors with low resistances (ranking from $R_{\text{cal}} \simeq 2\Omega$ to 7Ω, see Figure 30). Since now the tolerance on the calibrating resistances is about $\pm 0.05\%$ the plot of Figure 30.b shows that the accuracy of the sensor in sea water is about $\pm 0.1\%$ which has to be compared to the $\pm 0.02\%$ in fresh water. However, this reduction of accuracy still ensures a detection range about the sensor length. This slight deterioration of the sensor performance is due to the influence of noise which increases with the decrease of R_{ext}. This is illustrated on Figure 31, which displays the ex-situ noise distribution (on Fig. 31.a with a calibration resistor of $R_{\text{cal}} \simeq 4.04\Omega$), the same distribution but in sea water with gantry's motors switched off (Figure 31.b), and with the motors switched on (Figure 31.c). The increase of noise is essentially due to the decrease of the voltage generator V_{IN} in (9). If one want to maintain exactly the same range as in the fresh water, a direct way would be to redesign the electronics with a generator capable of generating a high current for a reasonable voltage. Thus, on a robot we could have two electronics, one for fresh water, the other for sea water, with the ability to switch from ones to the others. Another solution consists in changing the geometry of the sensor in order to increase its external resistance (the S_o matrix of section II.A) in the absence of any object. This is the case of the design of the robot presented in section 8, where the size of electrodes is dramatically reduced with respect to the area of the insulating boundaries.

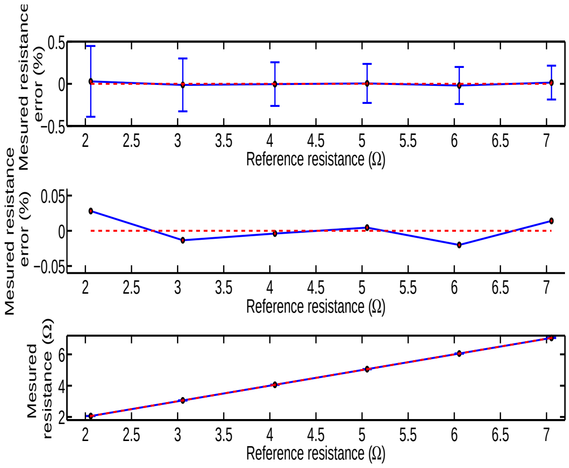

FIGURE 30 – Calibration of one channel of the receiving electronics.

7.7 Comparison with the Model

Using the analytical model in section II, which is, unlike the BEM, usable in real-time, we then compared the predictions of the model with the experimental data in the case of a simple scene. The two-electrode probe made a wall to wall movement, passing within 50 mm of an insulating sphere of 40 mm diameter. In Fig. 32, we have presented experimental results (circles) as well as theoretical predictions (plain and dashed curves) for $\gamma = 359$ μS/cm±1 μS/cm, accordingly to the precision available on the conductivity measurements.

The model turns out to be in rather good agreement with the data, although one observes a systematic deviation of the order of 1.5% which exceeds the error made on conductivity measurements. The remaining (small) discrepancy could be due to effects not taken into account in the physical modeling, such as the contact impedance between the electrodes and the conductive medium [27]. Very good agreement with the experimental data is obtained by adopting an effective value of the conductivity γ of 354 μS/cm. This result suggests that such a sensor can be used for real-time underwater electrolocation based on simple analytical models as in a Kalman filtering based approach [28, 29].

8 Future Robot Project

Beyond these first results obtained on the electrolocation testbed, we are actually building a first reconfigurable underwater robot equipped with this electrolocation sensor. This robot is planned in the context of the European project Angels [13] whose goal is the design of an eel-like robot composed of nine connected rigid modules equipped with electric sense. Thanks to its ability to change its morphology, this robot would be well adapted to exploration missions or object recognition in confined spaces. When all the modules are joined together, the robot will swim like an eel to minimize energy consumption. When detached, each module will benefit from the same electronics as our slender probes. An image of one module of the robot is depicted in Fig. 33. It consists of an insulating shell on which are fixed small hemispherical electrodes. As regards locomotion, it is achieved by two axial propellers fixed to the top and the bottom of the module while a third (lateral) propeller is located inside a transverse hole crossing the module from side to side.

To relate the sensor range to the dynamic performance of the modules, one considers the simple scenario where a module goes forward perpendicularly to a wall with a maximal thrust :

$$\overline{T}_+ = \frac{\rho}{2} C_d A v_c^2, \tag{14}$$

and tries to avoid collision by inverting the thrust. In (14), ρ is the volume mass of water, C_d the dimensionless axial drag coefficient of the module, A is the area offered by the module to the flow, while v_c is the maximal cruising forward velocity. In the case of the robot of Fig. 33, the shape is quasi-ellipsoidal with a length $L = 0.25$m, a height of 0.11m and a width of 0.055m, while the propellers are such that $\overline{T}_+ = 0.3N$. Thus (14) gives $v_c \simeq 0.3$m/s with a Reynolds number $R_e \simeq 5.10^4$. Then, introducing (14), into the axial dynamic balance of one module, allows one to evaluate the minimal counterthrust $\overline{T}_-$ required to reach the wall with a null velocity, while starting from a maximal velocity v_{max} :

$$\overline{T}_- = \frac{\lambda v_{max}^2}{e^{(2\lambda d/m)} - 1}, \tag{15}$$

where d denotes the sensor range, m $(= 1.3$kg), is the virtual (solid + added) axial mass of the module while $\lambda = (1/2)\rho A C_d$ $(= 3$kg/m). Thus, d $(= L = 0.3$m) and $\overline{T}_-$ $(= \overline{T}_+ = 0.3$N, the propellers are symmetric) being imposed by the intrinsic capabilities of the actuators and the sensor, (15) allows evaluating v_{max}. In the case of the project's robot, we have $v_{max} \simeq 0.5$m/s (1.8km/h) which is higher than the (maximal) cruising speed given by (14). In fact, the minimal range of detection beyond which collision is avoided is $\underline{d} = L/2$. As a result, though there are other delays, as those introduced by the propellers dynamics, the range of the sensor should not limit too much the intrinsic dynamic performance of the actuators.

9 Conclusion

We have presented the first results obtained on a practicable electrolocation system devoted to robotics. With electrodes arrayed on a realistic slender body, the sensor surpasses the idealized point electrode device of [12]. Measurement accuracy was challenging as object detection requires measurement of a very low relative perturbation (of the order of 1/1000), but this was achieved in our work on the electronics. As a consequence, our first experimental results based on current measurement showed a good sensitivity to the presence of objects. Finally, the proposed electronics allow reproducing the range of the fish. Thus, in the perspective of underwater robotics, being of one length of the body (in fact the maximum length of a dipole attached to the body), the expected range is one meter for a one meter length vehicle, ten meters for a ten meters length vehicle and so on (according to (5)). We have dealt with the problem of the perturbation caused by variations in the fluid conductivity by introducing an embarked conductivity meter for real-time and local measurement of this quantity and will transpose this solution to our future robot. However, the sensitivity of the sensor to other sources of conductivity variations (than electric colors of materials) can also be a useful complement to other sensors, in order to detect gradients of other nature, as chemical or thermic ones. As regards control aspects, several control techniques have been experimented on the sensor to demonstrate its exploitability for robotics applications and will be presented in future articles [28, 29, 30]. Some of them use models while others are model-free approaches known as reactive approaches [31]. These reactive approaches are well adapted to obstacle avoidance or object following depending on their electric conductivity with respect to the ambient medium. Finally, several extensions of the sensor are currently in progress. First, other measurement modes as the active or passive voltage measurements named $I - U$ or $0 - U$ modes ("0" meaning that there is no current emission from the sensor), or the passive current measurement mode $0-I$, are now being explored, with the ability to combine them and even to switch between them. Second, we are also developing electronics allowing to switch between emitters and receivers (a feature referred to as "reconfigurability") in order to shape the basal electric field in real-time. To date, the $U-I$ sensor here presented, is in course of implementation on the modules of the Angels project. First experiments show that thanks to a reactive controller, an autonomous module can follow a conductive target. As regards submarine robotics, the article also addresses the problem of electrolocation in salty water. In this context in spite of the decrease of the external resistance of two orders of magnitude, the electronics proposed in the article still works with a new calibration. Thus, for an underwater vehicle, we could combine two circuits, one designed for salty and the other for fresh waters with the possibility to switch from one to the other. Finally, while the article considers the case of a slender geometry, other designs, with more bulky shapes and smaller electrodes tend to compensate the high conductivity of salty waters. Lastly, in spite of these encouraging results, many things remain to do before equipping an operational underwater vehicle with this new sensor. In this perspective, the exploitation of the individual advantages of the different measurement modes ($U-I$, $I-I$, $0-I$, $U-U$...), seems a promising way to improve the performance of electric perception as a whole. For instance, $I-I$ mode could offer the advantage to make electrolocation independent of the water conductivity, while $U-U$ mode could be better to increase the number of electro-receptors.

Acknowledgment

The ANGELS project is funded by the European Commission, Information Society and Media, Future and Emerging Technologies (FET) contract number : 231845. The authors gratefully acknowledge the reviewers' comments, and thank Douglas Carnall for his careful proofreading of this manuscript.

Références

[1] H. Lissmann and K. Machin, "The mechanism of object location in gymnarchus niloticus and similar fish," *The Journal of Experimental Biology*, no. 35, pp. 451–486, 1958.

[2] K. Shieh, W. Wilson, M. Winslow, D. McBride, and C. Hopkins, "Short-range orientation in electric fish - an experimental study of passive electrolocation." *Journal of Experimental Biology*, vol. 199, pp. 2383–2393, 1996.

[3] B.Rasnow and J. M. Bower, "The electric organ discharges of the gymnotiform fishes," *Journal of Comparative Physiology A*, vol. 178, no. 3, pp. 383–396, 1996.

[4] D. Babineau, A. Longtin, and J. Lewis, "Modeling the electric field of weakly electric fish," *The Journal of Experimental biology*, vol. 209, pp. 3636–3651, 2006.

[5] M. MacIver, N. Sharabash, and M. Nelson, "Prey-capture behavior in gymnotid electric fish : motion analysis and effects of water conductivity," *The Journal of Experimental Biology*, vol. 204, pp. 543–557, 2001.

[6] B.Rasnow, "The effects of simple objects on the electric field of apteronotus," *Journal of Comparative Physiology A*, vol. 178, no. 3, pp. 397–411, 1996.

[7] A. Caputi, R. Budelli, and C. Bell, "The electric image in weakly electric fish : physical images of resistive objects in gnathonemus petersii," *Journal of Experimental Biology*, vol. 201, no. 14, pp. 2115–2128, 1998.

[8] G. V. D. Emde, S. Schwarz, L. Gomez, R. Budelli, and K. Grant, "Electric fish measure distance in the dark," *Letters to Nature, Nature*, vol. 395, pp. 890–894, 1998.

[9] G. Emde, "Active electrolocation of objects in weakly electric fish," *The Journal of Experimental Biology*, vol. 202, pp. 1205–1215, 1999.

[10] M. MacIver and J. Solberg, "Towards a biorobotic electrosensory system," *Autonomous robots*, vol. 11, pp. 263–266, 2001.

[11] J. Solberg, K. Lynch, and M. MacIver, "Active electrolocation for underwater target localization," *The International Journal of Robotics Research*, vol. 27, pp. 529–548, 2008.

[12] ——, "Robotic electrolocation : Active underwater target localization," *International Conference on Robotics and Automation*, pp. 4879–4886, 2007.

[13] The ANGELS' project, http ://www.theangelsproject.eu.

[14] B. Jawad, P. Gossiaux, F. Boyer, V. Lebastard, F.Gomez, N.Servagent, S.Bouvier, A.Girin, and M.Porez, "Sensor model for the navigation of underwater vehicles by the electric sense," in *Robotics and Biomimetics ROBIO IEEE*, 2010, pp. 879–884.

[15] F. Boyer, P. Gossiaux, B. Jawad, V. Lebastard, and M.Porez., "Model for a sensor inspired by electric fish," *IEEE transactions on robotics*, vol. 28, no. 2, pp. 492–505, 2012.

[16] J. Jackson, *Classical Electrodynamics.* John Wiley & Sons, New York, 1962.

[17] L. Gaul, M. Kögl, and M. Wagner, *Boundary element methods for engineers and scientists.* Springer-Verlag, 2003.

[18] Y.Liu, *Fast multipole boundary element method.* Cambridge university press, 2009.

[19] M. Porez, V. Lebastard, A. J. Ijspeert, and F. Boyer, "Multy-physics model of an electric fish-like robot : Numerical aspects anbd application to obstacle avoidance," in *IEEE/RSJ Int. Conf. on Intelligent Robots and Systems*, 2011, pp. 1901–1906.

[20] J.-P. Diard and B. L. G. C. Montella, *Cinétique électrochimique.* Hermann (Paris), 1996.

[21] L. A. Klein and C. T. Swift, "An improved model for the dielectric constant of sea water at microwave frequencies," *IEEE Trans. Ant. Prop.*, vol. AP-25, pp. 104–111, 1977.

[22] W. Ellison, A. Balana, G. Delbos, K. Lamkaouchi, L. Eymard, C. Guillou, and C. Prigent, "New permittivity measurements of seawater," *Radio Science*, vol. 33, pp. 639–648, 1998.

[23] D. P. Fernandez, Y. Mulev, A. Goodwin, and J. L. Sengers, "A database for the static dielectric constant of water and steam," *J. Phys. Chem. Ref. Data*, vol. 25, no. 1, pp. 1291–1306, 1995.

[24] T. Vilhunen, J. P. Kaipio, P. J. Vauhkonenand, T. Savolainen, and M. Vauhkonen, "Simultaneous reconstruction of electrode contact impedances and internal electrical properties : I. theory," *Meas. Sci. Technol.*, vol. 13, pp. 1848–1854, 2002.

[25] A. Charoy, *Parasites et perturbations des électroniques.* Dunod, 1996.

[26] G. Vasilescu, *Bruits et signaux parasites.* Dunod, 1999.

[27] E. Somersalo, M. Cheney, and D. Isaacson, "Existence and uniqueness for electrode models for electric current computed tomography," *SIAM J. Appl. Math.*, vol. 52, pp. 1023–1040, 1992.

[28] V. Lebastard, C. Chevallereau, A. Amrouche, B. Jawad, A. Girin, F. Boyer, and P. Gossiaux, "Underwater robot navigation around a sphere using electrolocation sense and kalman filter," in *IROS 2010 IEEE*, 2010, pp. 4225–4230.

[29] V. Lebastard, C. Chevallereau, A. Girin, N. Servagent, P. Gossiaux, and F. Boyer., "Reconstruction and navigation with electric sense based on kalman filtering," *The International Journal of Robotics Research.*, 2011 (submitted).

[30] F. Boyer, V. Lebastard, C. Chevallereau, and N. Servagent, “Underwater reflex navigation in confined environment based on electric sense,” *IEEE transactions on robotics*, 2012 (submitted).

[31] R. Brooks, “Intelligence without representation,” *Artificial Intelligence*, vol. 47, pp. 139–159, 1991.

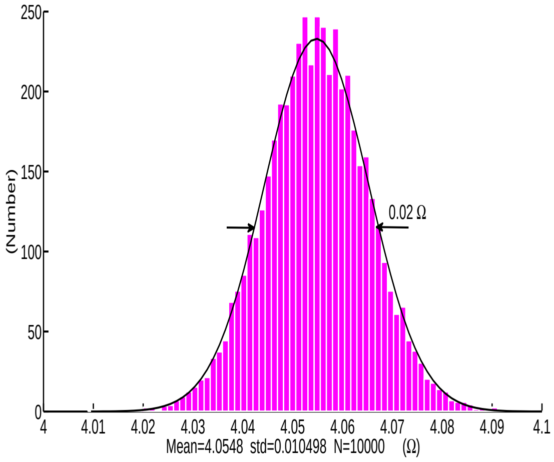

(a) standard resistor $R_{\rm cal} = 4\ \Omega$

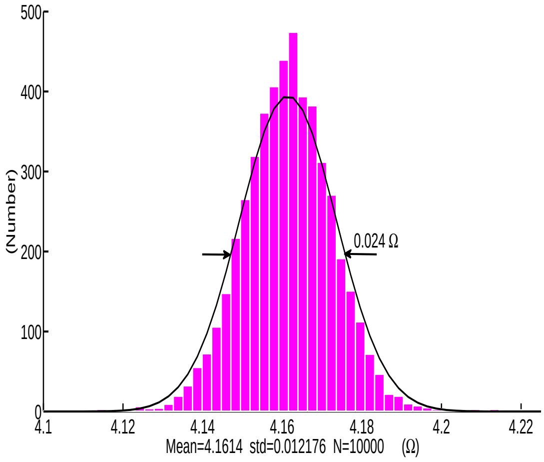

(b) Probe resistance in sea water with motors off

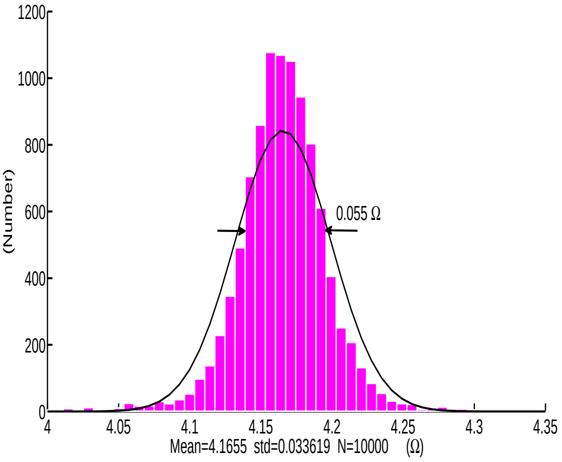

(c) Probe resistance in sea water with motors on

FIGURE 31 – Histogram : distribution of resistance measurements obtained with $U - I$ electronics for a population of $N = 10000$ individual measurements in sea water ; plain line : “best” gaussian fit, of same average and standard deviation as the distribution.

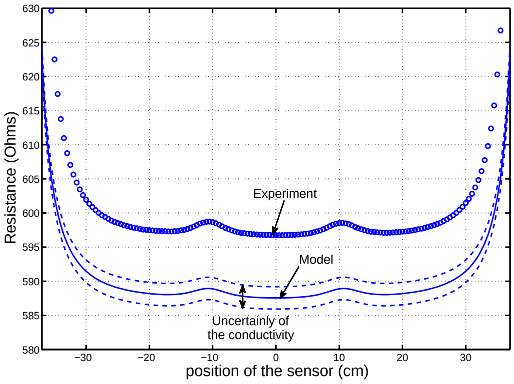

FIGURE 32 – Comparison between the the experimental data (circles) and the model ; plain line corresponds to the model evaluated with the measured conductivity value of $\gamma = 359$ μS/cm, while dashed lines correspond to $\gamma = 358$ μS/cm and $\gamma = 360$ μS/cm, chosen to illustrate the effect of the conductivity meter accuracy (1 μS/cm) on the model predictions.

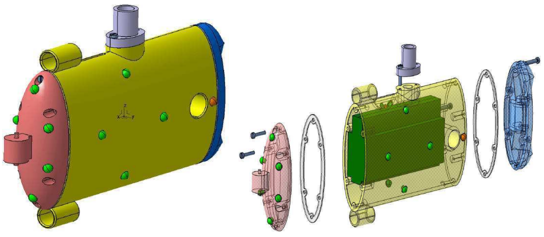

(a) overview

(b) View with electronic clutter (green).

FIGURE 33 – CAD view of the ANGELS-v1 module, designed by the CRIM Lab of Scuola Superiore Sant'Anna. The attachment device on top will be removed in the final version and allows it to be studied on the gantry of the tank.